RSC Advances

PAPER

View Article Online
View Journal | View Issue

Cite this: *RSC Adv.*, 2024, **14**, 21668

Exploration of the VEGFR-2 inhibition activity of phthalazine derivatives: design, synthesis, cytotoxicity, ADMET, molecular docking and dynamic simulation†

Hatem Hussein Bayoumi,[a] Mohamed-Kamal Ibrahim,[a] Mohammed A. Dahab,[a] Fathalla Khedr[a] and Khaled El-Adl *[ba]

Novel phthalazine derivatives were designed, synthesized and evaluated against Hep G2 and MCF-7 as VEGFR-2 inhibitors. In particular, compounds **2g** and **4a** were found to be the most potent derivatives among all the tested compounds against MCF-7 and Hep G2 cancer cell lines with IC_{50} values of 0.15 and 0.12 and 0.18 and 0.09 μM respectively. Moreover, compounds **3a**, **3c**, **5a** and **5b** displayed excellent anticancer activities against MCF-7 and Hep G2 cancer cell lines. The highly active derivatives **2g**, **3a**, **3c**, **4a**, **5a** and **5b** were evaluated for their inhibitory activities against VEGFR-2. The tested compounds displayed high to low inhibitory activities with IC_{50} values ranging from 0.148 to 0.892 μM. Among them, compounds **2g** and **4a** were found to be the most potent derivatives that inhibited VEGFR-2 with IC_{50} values of 0.148 and 0.196 μM respectively. Compounds **3a**, **3c**, **5a** and **5b** exhibited good activity with IC_{50} values of 0.375, 0.892, 0.548 and 0.331 μM respectively. Sorafenib was used as a reference drug in this study. Molecular modeling studies were carried out for all compounds against the VEGFR-2 active site. The data obtained from biological testing highly correlated with those obtained from molecular modeling studies. Moreover, MD simulation results indicated the stability of ligand–target interaction. Furthermore, our derivatives **2g** and **4a** showed a good *in silico* calculated ADMET profile.

Received 10th May 2024
Accepted 26th June 2024

DOI: 10.1039/d4ra03459g

rsc.li/rsc-advances

1. Introduction

Several phthalazine derivatives have been reported[1–7] as promising anticancer agents as they are potent inhibitors of VEGFR-2.[8–11] Phthalazine-1,4-diones have been reported as potent type II IMP dehydrogenase inhibitors and effective anti-proliferative agents against different human and murine tumor cells, particularly against hepatocellular carcinoma.[3] Moreover, 1,4-disubstituted phthalazines have attracted considerable attention as promising and effective anticancer agents.[3,5] In addition, many triazolo[3,4-*a*] phthalazine derivatives have been reported to have promising antitumor activities against MGC-803, EC-9706, HeLa and MCF-7 human cancer cell lines.[12]

Increasing attention has been paid to the synthesis of numerous phthalazines during the past two decades as they are favorable drug candidates for cancer treatment. Several research efforts were made that led to the discovery of numerous phthalazine derivatives with diverse enzymatic and cellular targets. For example, AMG 900 **I** (Fig. 1) was synthesized by Amgen as an orally bioavailable, potent, and highly selective pan-aurora kinase inhibitor that is active in taxane resistant tumor cell lines.[6] AMG 900 **I** was active in an AZD1152-resistant HCT116 variant cell line that harbors an aurora-B mutation (W221L).[7] Thereafter, Cee *et al.* discovered two selective and orally bioavailable pyridinyl-pyrimidine phthalazine aurora kinase inhibitors.[13] Vatalanib (PTK787) **II**[14] (Fig. 1) inhibits both VEGFR-1 and VEGFR-2 with IC_{50} of 380 and 20 nM, respectively. Vatalanib showed good oral absorption and *in vivo* anticancer activities against a panel of human cancer xenograft models; however, vatalanib is presently in phase III clinical trials for colorectal cancer treatment.[15,16] In addition, many anilino-phthalazines have been reported as potent inhibitors of VEGFR-2 as AAC789 **III** and IM-023911 **IV** with IC_{50} = 20 and 48 nM, respectively (Fig. 1).[8–11,17,18] VEGFR-2 inhibitors can be classified into three categories: type I inhibitors inhibit the ATP binding region forming a hydrogen bond with the hinge region amino acid Cys919; type II inhibitors occupy the ATP binding site and extend over the gate area into the adjacent allosteric hydrophobic pocket; and type III inhibitors block the allosteric hydrophobic pocket forming hydrophobic interactions.[19]

[a]*Pharmaceutical Medicinal Chemistry and Drug Design Department, Faculty of Pharmacy (Boys), Al-Azhar University, Nasr City 11884, Cairo, Egypt. E-mail: eladlkhaled74@yahoo.com; eladlkhaled74@azhar.edu.eg; khaled.eladl@hu.edu.eg*

[b]*Pharmaceutical Chemistry Department, Faculty of Pharmacy, Heliopolis University for Sustainable Development, Cairo, Egypt*

† Electronic supplementary information (ESI) available. See DOI: https://doi.org/10.1039/d4ra03459g

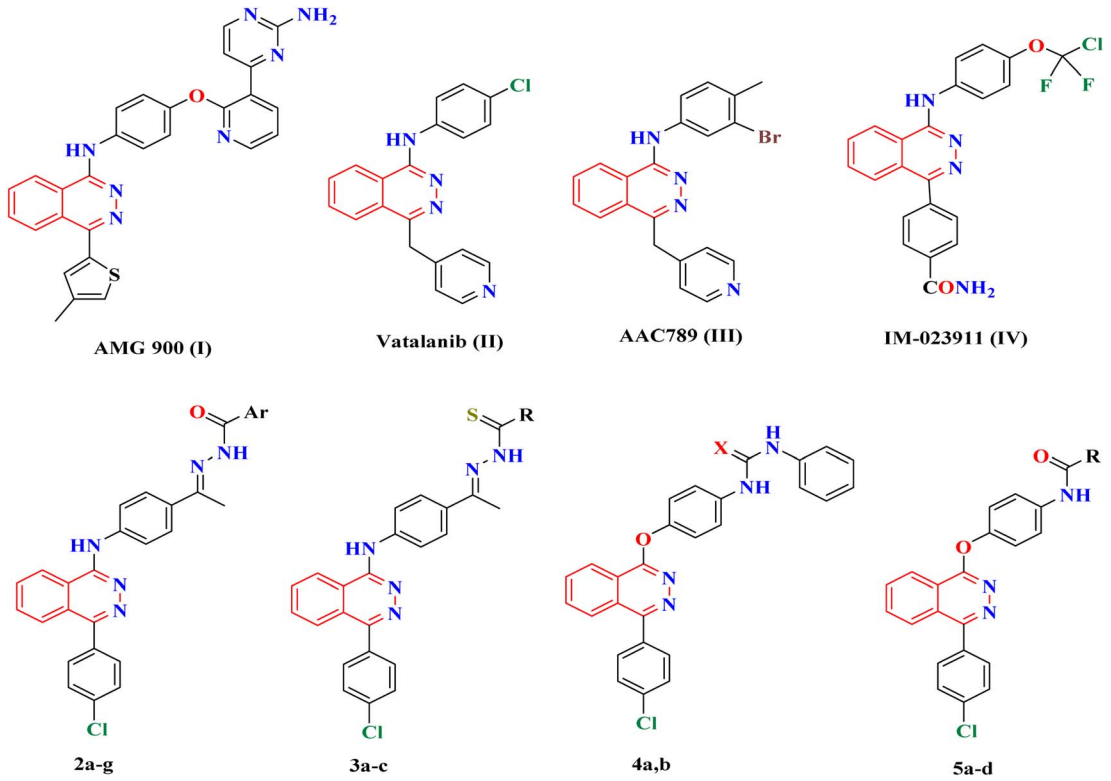

Fig. 1 Structures of the lead anticancer phthalazine derivatives I–IV and our designed derivatives.

In this context, a 1-substituted-4-phenylphthalazine scaffold, bearing different 4-substituted anilines and/or phenols, in particular, emerged as an interesting scaffold for designing VEGFR-2 inhibitors (Fig. 2). The abovementioned facts have aggravated us to design novel 4-phenylphthalazine derivatives in an attempt to obtain more potent anticancer agents. In continuation of our efforts to obtain new anticancer agents,[20–34] the goal of the present work was the synthesis of new agents with the same essential pharmacophoric features of the reported and clinically used VEGFR-2 inhibitors (*e.g.* vatalanib and sorafenib).

2. Results and discussion

2.1. Rationale and structure-based design

Our derivatives were designed based on the essential pharmacophoric features of VEGFR-2 inhibitors[20–23] (Fig. 2). We synthesized a series of new phthalazine derivatives encouraged by the bioisosteric modifications of VEGFR-2 inhibitor (sorafenib) at four different positions: (1) a flat heteroaromatic ring that occupies the ATP binding domain, (2) a central hydrophobic linker, (3) a spacer with a functional group that has both H-bond acceptor and donor properties to bind with key amino acids (Glu885 and Asp1046), and (4) a terminal hydrophobic moiety that fits into the allosteric hydrophobic pocket (Fig. 2).

2.2. Chemistry

The synthetic strategy for the preparation of target compounds (**2–5**) is depicted in Schemes 1 and 2. The synthesis was started by cyclocondensation of 2-(4-chlorobenzoyl)benzoic acid with hydrazine hydrate to afford the corresponding 4-(4-chlorophenyl)phthalazin-1(2*H*)-one, which underwent chlorination by reaction with phosphorous oxychloride to afford 1-chloro-4-(4-chlorophenyl)phthalazine.[3,4] The chloro derivative was refluxed with 4-aminoacetophenone to afford the corresponding acetyl derivative **1**, which underwent condensation with the appropriate acid hydrazide, namely, benzohydrazide, 2-bromobenzohydrazide, 2-chlorobenzohydrazide, 2-hydroxybenzohydrazide, 4-aminobenzohydrazide, nicotinohydrazide and/or isonicotinohydrazide to afford the corresponding hydrazone derivatives **2a–g** respectively. In addition, the acetyl derivative **1** was allowed to react with the appropriate thiosemicarbazide, 4-phenyl-3-thiosemicarbazide and/or methyl hydrazinecarbodithioate to give the corresponding derivatives **3a–c** respectively (Scheme 1). Furthermore, the intermediate 1-chloro-4-(4-chlorophenyl)phthalazine was reacted with the appropriate urea and/or thiourea to give the corresponding derivatives **4a,b** respectively. Moreover, it was reacted with the appropriate amide derivative to afford the corresponding acid amide derivatives **5a–d** respectively (Scheme 2).

2.3. *In vitro* anti-proliferative activity

The anti-proliferative activity of the newly synthesized phthalazine derivatives **2a–g**–**5a–d** was examined against two human tumor cell lines, namely, hepatocellular carcinoma (Hep G2) and breast cancer (MCF-7) using a 3-[4,5-dimethylthiazol-2-yl]-2,5-diphenyltetrazolium bromide (MTT) colorimetric assay, as described by Mosmann.[35–37] Sorafenib was used as a reference

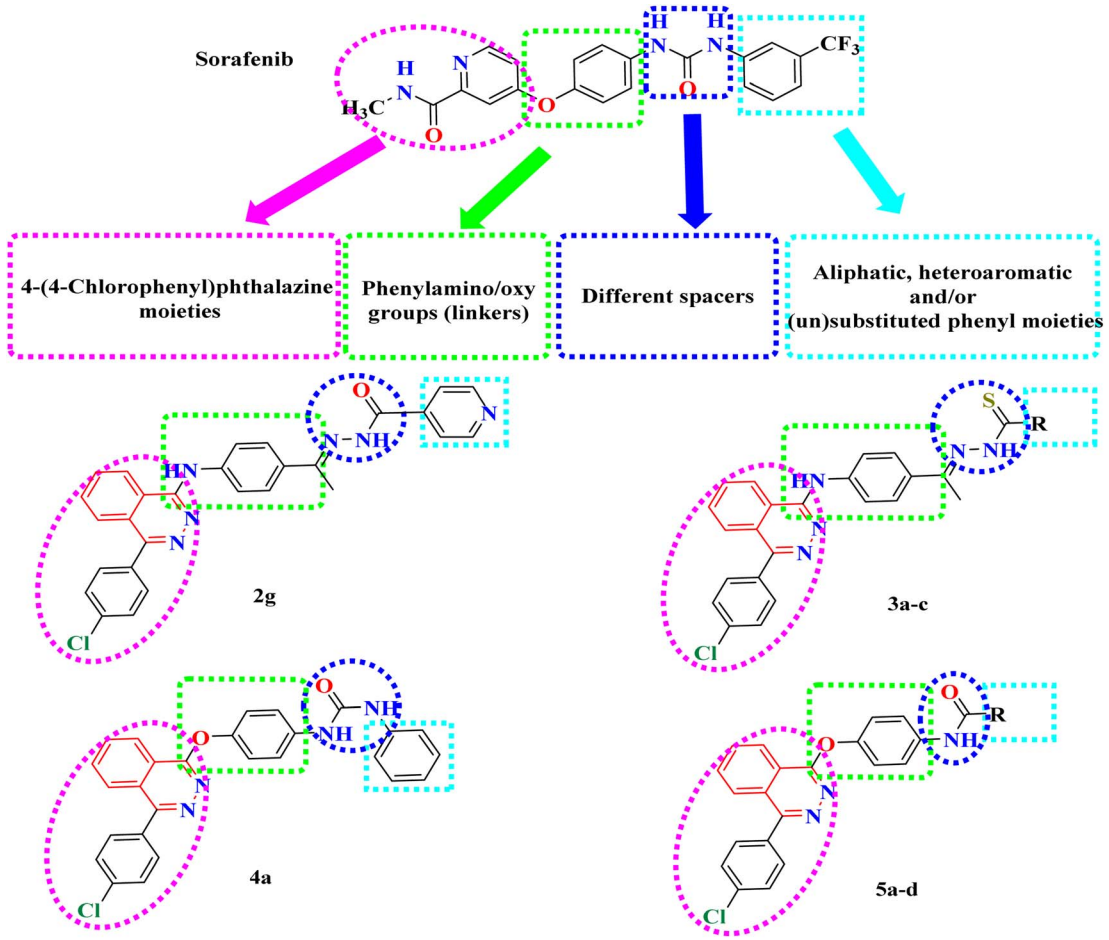

Fig. 2 Basic structural features of VEGFR-2 inhibitors.

cytotoxic drug (Table 1). From the obtained results, it was explicated that most of the prepared compounds displayed excellent to low growth inhibitory activity against the tested cancer cell lines. In particular, compounds **2g** and **4a** were found to be the most potent derivatives among all the tested compounds against the two MCF-7 and Hep G2 cancer cell lines with IC_{50} = 0.15, 0.12 and 0.18, 0.09 μM respectively.

With respect to the MCF-7 cell line, compounds **3a**, **3c**, **5a**, **5b** and **5c** displayed very good anticancer activities with IC_{50} ranging from 0.15 to 0.28 μM. Compounds **2b**, **2e**, **2f** and **3b**, with IC_{50} ranging from 0.71 to 0.98 μM, exhibited good cytotoxicity. Compounds **2a**, **2c**, **4b** and **5d**, with IC_{50} ranging from 1.12 to 1.74 μM displayed moderate cytotoxicity, while compound **2d** with IC_{50} 3.71 μM displayed the lowest cytotoxicity.

With respect to the Hep G2 hepatocellular carcinoma cell line, compounds **3a**, **3c**, **5a** and **5b** displayed very good anticancer activities with IC_{50} ranging from 0.18 to 0.26 μM. Compounds **2a**, **2b**, **2c** and **2f** with IC_{50} ranging from 0.59 to 0.77 μM exhibited good cytotoxicity. Compounds **2e**, **3b**, **4b**, **5c** and **5d** with IC_{50} ranging from 1.19 to 1.63 μM displayed moderate cytotoxicity, while compound **2d** with IC_{50} of 2.18 μM displayed the lowest cytotoxicity.

2.4. *In vitro* VEGFR-2 kinase assay

The highly active derivatives **2g**, **3a**, **3c**, **4a**, **5a** and **5b** were evaluated for their inhibitory activities against VEGFR-2 with an anti-phosphotyrosine antibody using an Alpha Screen system (PerkinElmer, USA).[38] Sorafenib was used as positive control in this assay. The tested compounds displayed high to low inhibitory activity with IC_{50} values ranging from 0.148 to 0.892 μM (Table 1) (Fig. 3). Among them, compounds **2g** and **4a** were found to be the most potent derivatives that inhibited VEGFR-2 at IC_{50} values of 0.148 and 0.196 μM respectively. Compounds **3a** and **5b** exhibited good activity with IC_{50} values of 0.375 and 0.331 μM respectively. Moreover, compound **5a** possessed moderate VEGFR-2 inhibition with an IC_{50} value of 0.548 μM. Finally, compound **3c** displayed the lowest VEGFR-2 inhibition with an IC_{50} value of 0.892 μM.

2.5. Structure–activity relationship (SAR)

The preliminary SAR study has focused on the effect of the hydrophobic and electronic nature of the substituents used in this study. Moreover, it focused on the effect of the type, length and number of spacers used and the distal moieties. The data obtained revealed that the tested compounds displayed different levels of anticancer activities. Generally, the 4-(4-

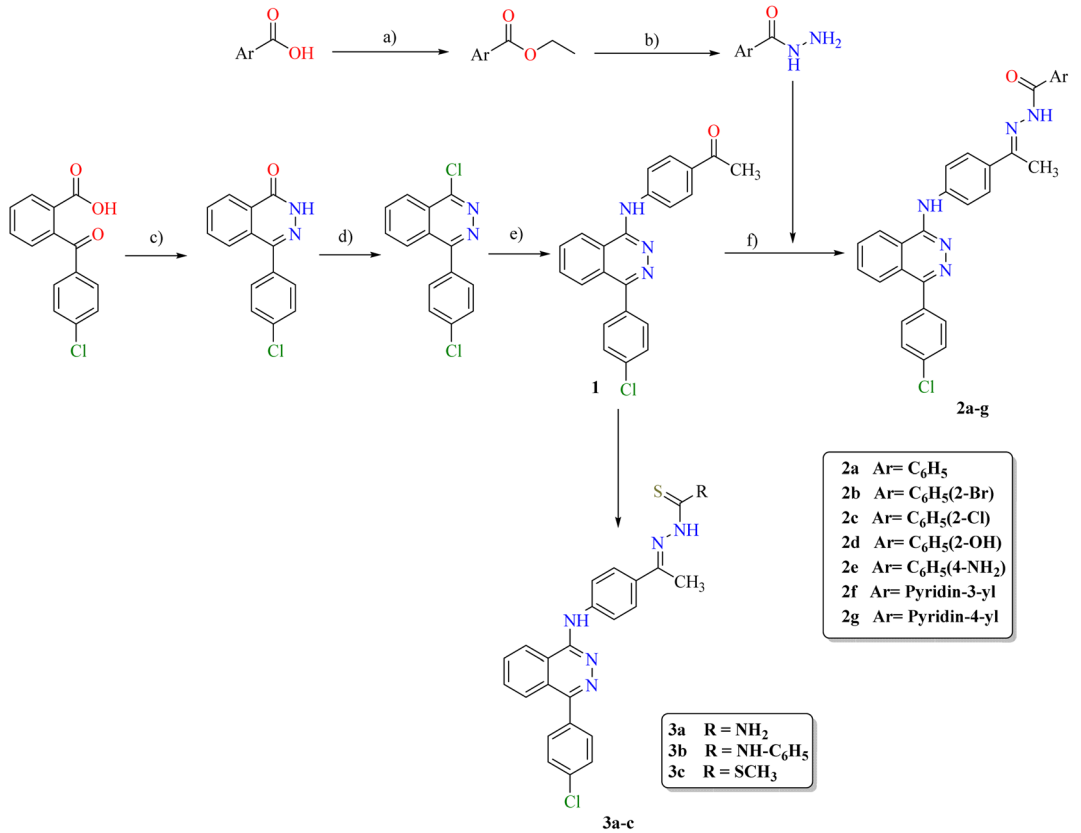

Scheme 1 Synthetic route for the preparation of the target compounds **2a–g** and **3a–c**.

chlorophenyl)phthalazine scaffold, bearing different 4-substituted anilines and/or phenols joined to the hydrophobic distal moieties through amide, hydrazide, thiosemicarbazide, urea and/or thiourea spacers containing (HBA–HBD). The lipophilicity and electronic nature of the distal moieties play an important role in VEGFR-2 inhibition and consequently the anticancer activities.

In molecular docking studies, the presence of the hydrazide and urea spacers, *e.g.* **2g** and **4a** respectively, impart a higher VEGFR-2 binding affinity and consequently higher anticancer activities. This higher affinity of such derivatives may be attributed to the increased length of the molecular structures so as to enable the distal moieties to occupy the hydrophobic grooves formed by Asp1046, Cys1045, Hie1026, Ile888, Ile892 and Glu885. Moreover, our derivatives containing a phthalazine heterocyclic ring that inhibits the ATP binding domain, form an H-bond with Cys919, and then extend over the gate area into the adjacent allosteric hydrophobic moiety, which confirmed our compounds as type II inhibitors of VEGFR-2.

From the structure of the synthesized derivatives and the data shown in Table 1, we can divide these tested compounds into three groups. The first group contains acid hydrazide spacers as in compounds **2a–g**. Generally, in this group, the derivative **2g** with an isonicotinohydrazide spacer exhibited the highest anticancer activities through this group against both Hep G2 and MCF-7 tested cell lines. Compound **2e** with the spacer benzohydrazide substituted at position-4 with the hydrophilic electron-donating NH_2 group showed higher anticancer activities than those of compound **2f** with isonicotinohydrazide and compound **2b** with benzohydrazide substituted at position-2 with the hydrophobic electron-withdrawing Br one against MCF-7 cell lines, while against Hep G2, the order of activity is the reverse as follows: **2b** > **2f** > **2e**. Moreover, compound **2b** with the more hydrophobic electron-withdrawing Br group at position-2 displayed higher anticancer activities than those of **2a** (unsubstituted benzohydrazide), **2c** with the hydrophobic electron-withdrawing Cl and **2d** with the hydrophilic electron-donating OH group against MCF-7 cell lines, while against Hep G2, the order of activity is **2c** > **2b** > **2a** > **2d**.

The second group **3a–c** contains thiosemicarbazide and hydrazinecarbodithioate spacers. Compound **3a** with a thiosemicarbazide spacer exhibited higher activities than those of compound **6** with a hydrazine carbodithioate spacer attached to the methyl group and **3c** with thiosemicarbazide attached to the phenyl group against both the Hep G2 and MCF-7 cell lines.

The third group comprises compounds **4a,b** and **5a–d** that contain urea, thiourea and/or amide spacers. In this group,

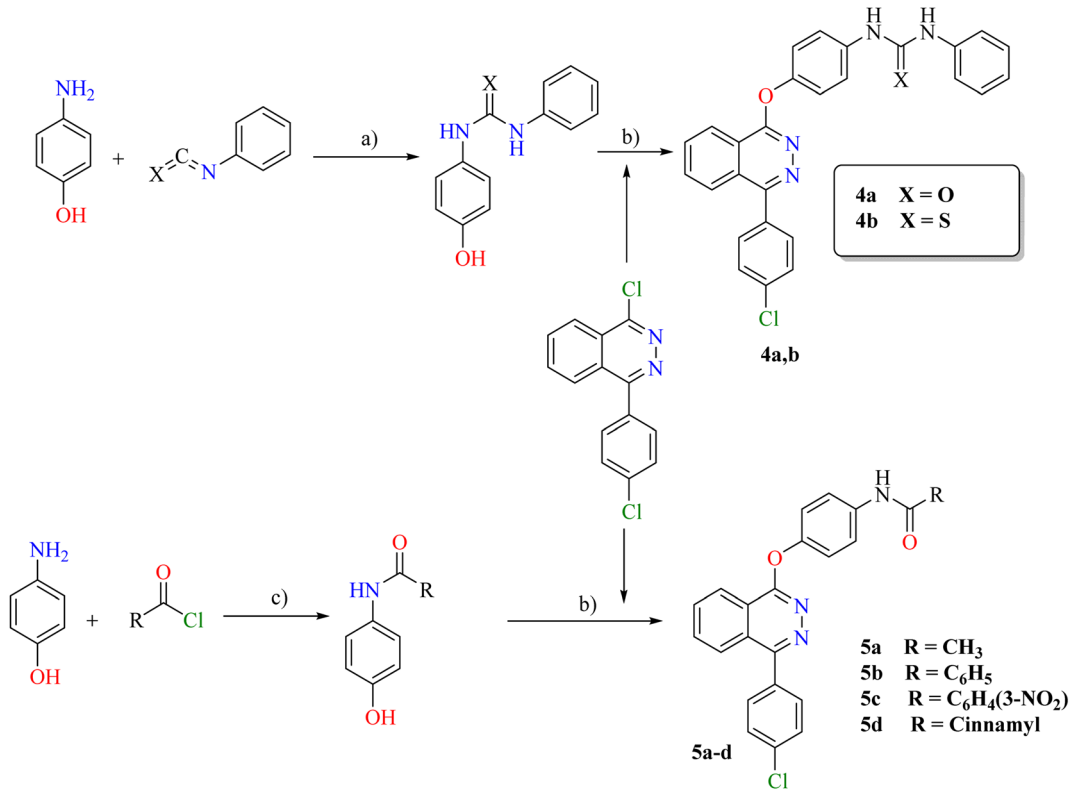

Scheme 2 Synthetic route for the preparation of the target compounds **4a,b** and **5a–d**.

Table 1 *In vitro* cytotoxic activities of the newly synthesized compounds against Hep G2 and MCF-7 cell lines and VEGFR-2 kinase assay

	IC_{50}[a] (μM)		
Compound	MCF-7	Hep G2	VEGFR-2
2a	1.55 ± 0.01	0.77 ± 0.01	NT[b]
2b	0.98 ± 0.01	0.63 ± 0.01	NT[b]
2c	1.74 ± 0.01	0.59 ± 0.01	NT[b]
2d	3.71 ± 0.07	2.18 ± 0.03	NT[b]
2e	0.71 ± 0.02	1.19 ± 0.04	NT[b]
2f	0.78 ± 0.01	0.75 ± 0.01	NT[b]
2g	0.15 ± 01	0.12 ± 0.01	0.148 ± 0.01
3a	0.18 ± 01	0.18 ± 01	0.375 ± 0.01
3b	0.87 ± 0.02	1.53 ± 0.06	NT[b]
3c	0.28 ± 01	0.20 ± 01	0.892 ± 0.13
4a	0.18 ± 01	0.09 ± 0.01	0.196 ± 0.01
4b	1.52 ± 0.01	1.63 ± 0.03	NT[b]
5a	0.18 ± 01	0.26 ± 01	0.548 ± 0.02
5b	0.15 ± 01	0.22 ± 01	0.331 ± 0.01
5c	0.18 ± 01	1.37 ± 0.14	NT[b]
5d	1.12 ± 0.02	1.26 ± 0.03	NT[b]
Sorafenib	0.05 ± 0.01	0.03 ± 0.01	0.059 ± 0.01

[a] IC_{50} values are the mean ± S.D. of three separate experiments. [b] NT = not tested.

compound **5b** with a benzamide spacer displayed higher activities than those of **4a** with phenylurea, **5a** with acetamide, **5c** with 3-nitrobenzamide, and **5d** with cinnamamide against MCF-7 cell lines, but against Hep G2, the order of activity is **4a** > **5b** > **5a** > **5d** > **5c** > **4b**.

2.6. Docking studies

All modeling experiments in the present work were performed using the Molsoft software. Each experiment used VEGFR-2 downloaded from the Brookhaven Protein Databank (PDB ID 4ASD).[39]

Sorafenib suggested binding mechanism produced 5 H-bonds and an energy value of −99.50 kcal mol^{-1} (Table 2). It generated 2 hydrogen bonds with Cys919 (2.51 Å and 2.10 Å), two with Glu885 (1.77 Å and 2.75 Å), and one with Asp1046 (1.50 Å). The pocket created by Cys919, Phe918, Leu1035, Lys920, Glu917, Val848 and Leu840 was occupied by the *N*-methyl-picolinamide group. Additionally, the hydrophobic groove formed by Cys1045, Leu1035, Val916, Lys868, and Val848 was occupied by the central phenyl linker. Moreover, Cys1045, Asp1046, Hie1026, Ile888, Ile892 and Glu885 formed a hydrophobic channel that was occupied by the terminal 3-trifluromethyl-4-chlorophenyl group (Fig. 4). The urea spacer had a crucial part in the binding of the VEGFR-2 enzyme, but it also played a crucial role in the high binding affinity of **Sorafenib**. These results encourage us to experiment with various spacers in order to obtain efficient VEGFR-2 inhibitors.

As planned, the proposed binding mode of compound **2g** is virtually the same as that of sorafenib. It showed −98.84 kcal mol^{-1} and formed 6 H-bonds with Cys919 (2.28 Å),

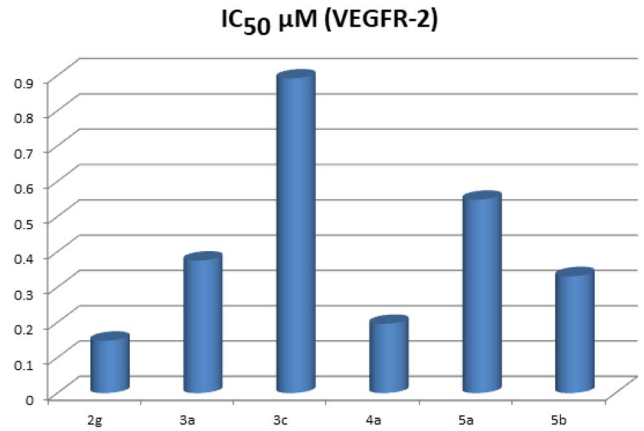

Fig. 3 IC_{50} (µM) of the tested compounds as VEGFR-2 inhibitors.

Table 2 Calculated free energies of binding (ΔG in kcal mol^{-1}) for the ligands

Compound	ΔG [kcal mol^{-1}]	Compound	ΔG [kcal mol^{-1}]
2a	−83.68	**3c**	−79.21
2b	−87.16	**4a**	−95.96
2c	−84.73	**4b**	−90.40
2d	−84.35	**5a**	−74.05
2e	−89.05	**5b**	−75.66
2f	−86.66	**5c**	−77.44
2g	−98.84	**5d**	−88.90
3a	−81.79	**Sorafenib**	−95.36
3b	−92.12		

Val916 (2.96 Å), Glu883 (2.68 Å), Asp1044 (1.78 Å and 1.95 Å) and Ile892 (2.95 Å). The 4-(4-chlorophenyl)phthalazine moiety occupied the hydrophobic pocket created by Cys919, Phe918, Leu1035, Lys920, Glu917, Val848 and Leu840. Additionally, the central phenyl linker occupied the hydrophobic groove formed by Cys1045, Leu1035, Glu917, Val916, Lys868, and Val848. Furthermore, the terminal pyridine ring occupied a hydrophobic channel formed by Asp1046, Hie1026, Ile888, Ile892 and Glu885 (Fig. 5). These interactions may explain the highest anticancer activities of compound **2g**.

The proposed binding mode of compound **4a** is virtually the same as that of **2g**. It showed −95.86 kcal mol^{-1} and formed 4 H-bonds with Cys919 (2.96 Å), Glu883 (2.05 Å and 2.95 Å), and Asp1044 (1.25 Å). The 4-(4-chlorophenyl)phthalazine moiety occupied the hydrophobic pocket created by Cys919, Phe918, Leu1035, Lys920, Glu917, Val848 and Leu840. Additionally, the central phenyl linker occupied the hydrophobic groove formed by Cys1045, Leu1035, Glu917, Val916, Lys868, and Val848. Furthermore, the terminal phenyl ring occupied a hydrophobic channel formed by Asp1046, Cys1045, Hie1026, Ile888, Ile892 and Glu885 (Fig. 6). These interactions of compound **4a** may explain its high anticancer activity.

The obtained results showed that our derivatives inhibited the ATP binding domain forming an H-bond with Cys919 and extended over the gate area into the adjacent allosteric hydrophobic moiety, which confirmed that our compounds were type II inhibitors of VEGFR-2.

2.7. Molecular dynamics simulation

The highly active derivatives **2g**, **3a**, **4a** and **5b** in the protein VEGFR-2 were simulated using molecular dynamics (MD). By utilizing Amber's MM/GBSA.py script and the trajectory, the receptor-ligand binding energy was calculated.[40] Additionally, sorafenib was used as a positive control. With the help of GAFF2[41,42] and the force field AMBERff14SB for the protein, ligand force fields were produced.[43] The monitored root-mean-

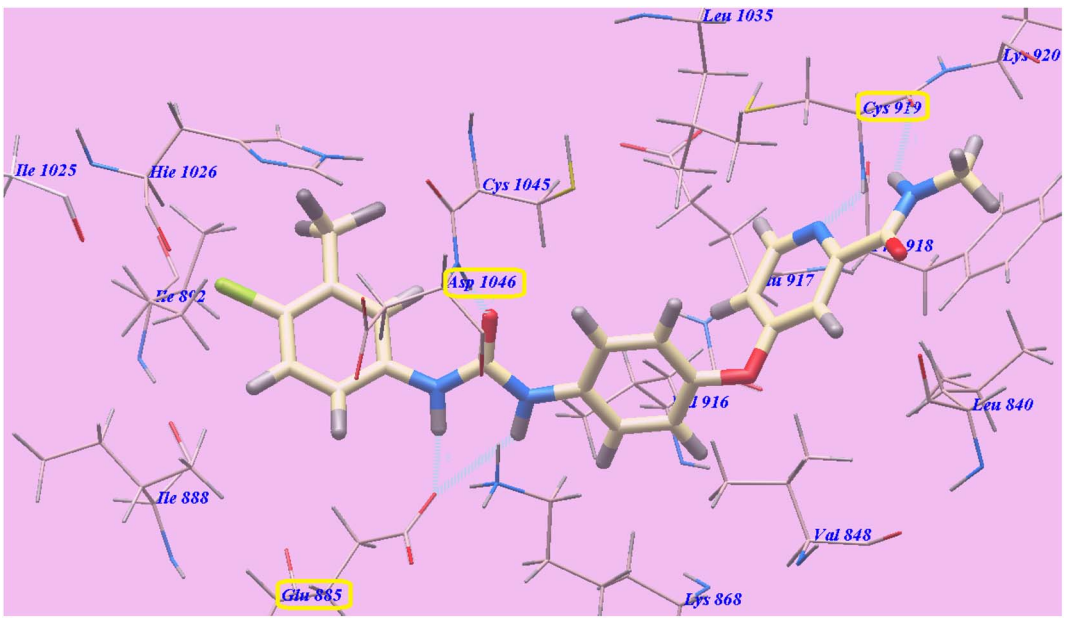

Fig. 4 **Sorafenib** predicted mechanism of binding with 4ASD. Dotted lines represent atoms that are H-bonded.

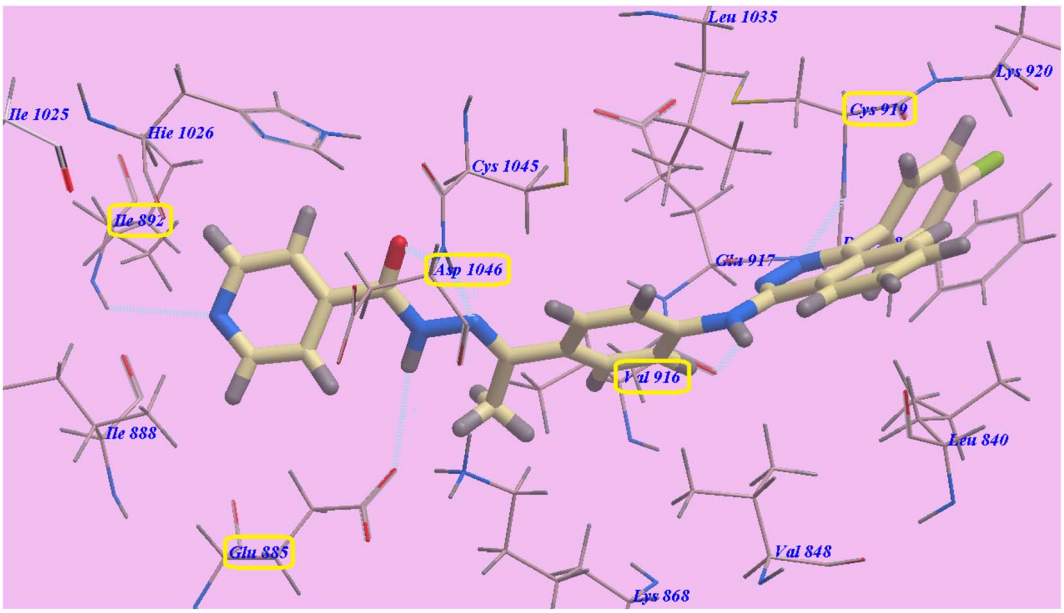

Fig. 5 Predicted binding mode for **2g** with 4ASD.

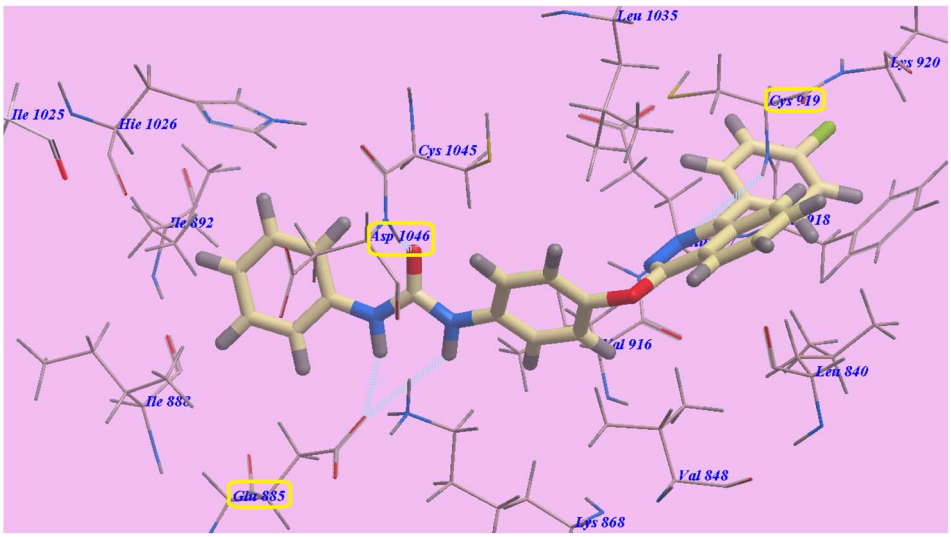

Fig. 6 Predicted binding mode for **4a** with 4ASD.

square deviation (RMSD) validated the studied inhibitor compounds' considerable global stability inside the target's recognized active site throughout the 50 ns all-atom MD runs (Fig. 7). A given ligand's molecular divergence from a defined original/reference structure was estimated using RMSD. The selected MD simulation procedure was valid, indicating the stability of the ligand–target interaction.

2.8. ADMET; *in silico* studies profile

An *in silico* study of the highly active derivatives **2g** and **4a** was conducted for their physicochemical character evaluation and the proposed ADMET profile. It was predicted using the pkCSM descriptor algorithm procedures[44] and matched to the rule of five described by Lipinski.[45] Good absorption properties were expected for the molecules that accomplish at least four rules: (i) no more than five hydrogen bond donors, (ii) no more than 10 hydrogen bond acceptors, (iii) molecular weight less than 500, and (iv) not more than 5 for log *P*. In the current work, the standard anticancer agent sorafenib and our new compounds **2g** and **4a** violate the log *P* rule.

As a result of obtaining data from Table 3, we can assume that compounds **2g** and **4a** have very good GIT absorption in humans (100 and 88.7 respectively), which indicates the different biological membranes to be easier to cross.[46] Therefore, they may show a significantly high bioavailability through GIT. Concerning CNS penetrability, our prepared compounds

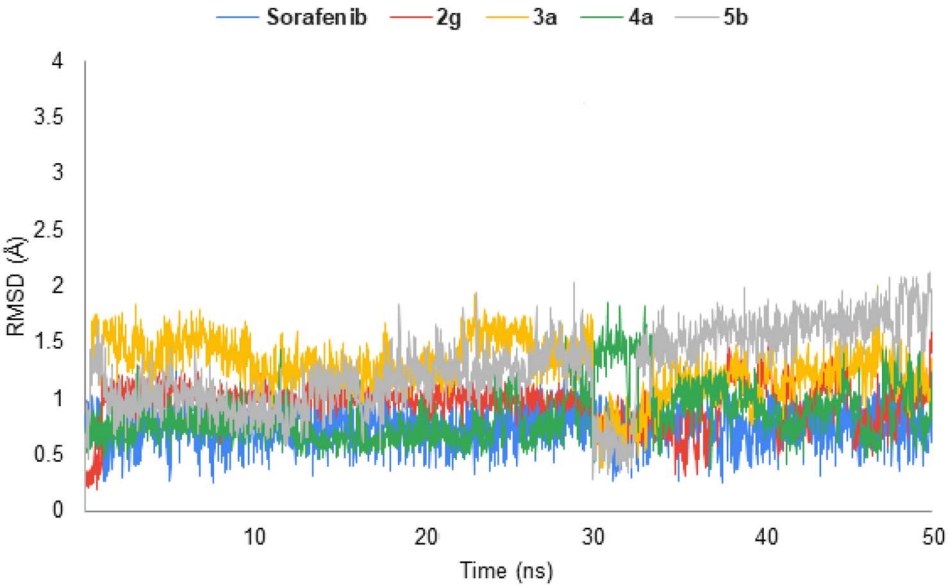

Fig. 7 Analysis of VEGFR-2 protein RMSD throughout 50 ns for the ligand–protein complexes.

Table 3 Highest effective compounds, sorafenib; ADMET profile

Parameter	2g	4a	Sorafenib
Physicochemical properties			
Molecular weight	492.97	466.928	464.831
log *P*	6.2428	7.3865	5.5497
Rotatable bonds	6	5	5
Acceptors	6	4	4
Donors	2	2	3
Surface area	212.437	200.735	185.111
Absorption			
Water solubility	−4.011	−3.562	−4.822
Human intest. absorption	100	88.707	89.043
Substrate for *P*-glycoprotein	+	+	+
Inhibitor of *P*-glycoprotein I	+	+	+
Inhibitor of *P*-glycoprotein II	+	+	+
Distribution			
Permeability throughout BBB	−0.478	−0.226	−1.684
Permeability to CNS	−1.713	−1.376	−2.007
Metabolism			
CYP2D6 substrate	−	−	−
CYP3A4 substrate	+	+	+
Inhibition of CYP1A2	+	+	+
Inhibition of CYP2C19	+	+	+
Inhibition of CYP2C9	+	+	+
Inhibition of CYP2D6	−	−	−
Inhibition of CYP3A4	+	−	+
Excretion			
Clearance	−0.167	−0.23	−0.219
Toxicity			
Human max. tolerated dose	0.367	0.515	0.549
Acute toxic activity (LD_{50})	3.12	3.665	2.538
Chronic toxic activity (LOAEL)	1.177	2.182	1.198
Hepatotoxic effect	+	+	+

can reach CNS (CNS permeability values −1.713 and −1.376 respectively), more than that of sorafenib (−2.007).

It is well known that CYP3A4, the major drug-metabolizing enzyme, could be inhibited by sorafenib, and also our derivative **2g** but our derivative **4a** does not. Elimination was expected depending on the total clearance, which is a considerable factor in deciding dose intervals. The data showed that compound **2g** exhibited a lower clearance rate than that of sorafenib and our compound **4a**, which demonstrated high clearance values. Thus, it could be eliminated faster, and as a result, supposed to have shorter dosing intervals. Unlike sorafenib and **4a**, the prepared compound **2g** exhibited low clearance rate, which signifies a long duration of action and extended dosing intervals. Toxicity is the final ADMET profile studied factor. As presented in Table 3, sorafenib and the novel compounds **2g** and **4a** shared the drawback of unwanted hepatotoxic actions. Sorafenib and **4a** demonstrated high maximum tolerated dose. These involve the advantage of the broad therapeutic index of sorafenib and our derivative **4a** respectively. The oral acute toxic doses of the novel compound **2g** and **4a** are higher than that of sorafenib. Lastly, the oral chronic toxic dose of the novel compound **4a** is higher than that of sorafenib.

3. Conclusion

In summary, a new series of phthalazine derivatives have been designed, synthesized and evaluated for their anticancer activities against two human tumor cell lines, namely, hepatocellular carcinoma (Hep G2) and breast cancer (MCF-7) as VEGFR-2 inhibitors. All the tested compounds showed variable anticancer activities. The molecular modeling was performed to investigate the binding mode of the proposed compounds with the VEGFR-2 active site. The data obtained from biological testing highly correlated with those obtained from molecular modeling studies. In particular, compounds **2g** and **4a** were

found to be the most potent derivatives among all the tested compounds against the two MCF-7 and Hep G2 cancer cell lines with $IC_{50} = 0.15$, 0.12 and 0.18, 0.09 μM respectively. Moreover, compounds **3a**, **3c**, **5a** and **5b** displayed very good anticancer activities against the two MCF-7 and Hep G2 cancer cell lines. The highly active derivatives **2g**, **3a**, **3c**, **4a**, **5a** and **5b** were evaluated for their inhibitory activities against VEGFR-2. The tested compounds displayed high to low inhibitory activities with IC_{50} values ranging from 0.148 to 0.892 μM. Among them, compounds **2g** and **4a** were found to be the most potent derivatives that inhibited VEGFR-2 at IC_{50} values of 0.148 and 0.196 μM respectively. Compounds **3a**, **3c**, **5a** and **5b** exhibited good activity with IC_{50} values of 0.375, 0.892, 0.548 and 0.331 μM respectively. Sorafenib was used as a reference drug in this study. Moreover, MD simulation procedure was valid, indicating the stability of the ligand–target interaction. Moreover, our derivatives **2g** and **4a** showed a good *in silico* calculated ADMET profile in comparison to sorafenib.

4. Experimental

4.1. Chemistry

All melting point tests were carried out by an open capillary method using a Stuart melting point apparatus SMP30 and were uncorrected. The infrared spectra were recorded using a Bruker FT/IR Spectro-photometer at Microanalytical Unit, Faculty of Science, Cairo University, and expressed in wave number (cm^{-1}). The ^1H NMR spectra were recorded at 400 MHz, while ^{13}C NMR spectra were run at 101 MHz, using a Bruker 400 MHz-NMR spectrophotometer at Nuclear Magnetic Unit, Faculty of Pharmacy, Mansoura University. Some of the ^1H NMR spectra were recorded at 300 MHz at Micro Analytical Unit, Faculty of Science, Cairo University. Chemical shifts were expressed in δ (ppm) and recorded relative to the (DMSO-d_6) solvent, using TMS as an internal reference standard. All coupling constant (J) values are given in Hertz. The mass spectra were recorded using a Varian MAT 311-A (70 e.v.) at the Regional Center for Mycology and Biotechnology, Faculty of Science, Al-Azhar University. Elemental analyses were performed at the Regional Center for Mycology and Biotechnology, Faculty of Science, Al-Azhar University. All compounds were within ±0.4 of the theoretical values.

4-(4-Chlorophenyl)phthalazin-1(2*H*)-one and 1-chloro-4-(4-chlorophenyl)phthalazine were obtained according to the reported procedures.[3,4]

4.1.1. General procedure for the synthesis of 1-(4-[{4-(4-chlorophenyl)phthalazin-1-yl}amino]phenyl)ethan-1-one (1). To a 150 ml round-bottom flask with a magnetic stirrer containing 1-chloro-4-(4-chlorophenyl)phthalazine (2.74 g, 0.01 mol) in 50 ml isopropanol, 4-aminoacetophenone (1.35 g, 0.01 mol) was added, stirred and refluxed for 3 h. A yellow solid was obtained, cooled, filtered, dried and crystallized from absolute ethanol to give the target compound **1**.

Yield, 80%; mp 176–8 °C; $IR_{\nu_{max}}$ (cm^{-1}): 3426 (NH), 3049 (C–H aromatic), 2915 (C–H aliphatic), 1679 (C=O), 1592 (C=N); ^1H NMR (400 MHz, DMSO-d_6) δ 10.69 (s, 1H), 8.20 (d, J = 8.3 Hz, 1H), 8.16 (t, J = 7.8 Hz, 1H), 8.09 (d, J = 8.4 Hz, 3H), 8.03 (d, J = 8.5 Hz, 2H), 7.97 (d, J = 8.2 Hz, 1H), 7.75 (d, J = 8.2 Hz, 2H), 7.71 (d, J = 8.2 Hz, 2H); ^{13}C NMR (101 MHz, DMSO-d_6) δ 197.26, 153.14, 152.61, 142.96, 136.17, 135.41, 133.62, 132.45, 130.51, 129.99, 129.50, 127.57, 125.45, 122.74, 121.61, 27.13; MS (*m*/*z*): 375.0982 (M^+ +2, 2.72%), 373.0982 (M^+, 8.13%), 79.04 (100%, base peak); Anal. calcd for $C_{22}H_{16}ClN_3O$ (373.84): C, 70.68; H, 4.31; N, 11.24. Found: C, 70.51; H, 4.43; N, 11.45%.

4.1.2. General procedure for the synthesis of *N′*-(1-[4-{(4-[4-chlorophenyl]phthalazin-1-yl)amino}phenyl]-ethylidene) substitutedhydrazide (2a–g). To a 100 ml round-bottom flask with a magnetic stirrer compound (**1**) (3.73 g, 0.01 mol) was added in 50 ml absolute ethanol. Then appropriate acid hydrazides, namely, benzohydrazide, 2-bromobenzohydrazide, 2-chlorobenzohydrazide, 2-hydroxybenzohydrazide, 4-amino-benzohydrazide, nicotinohydrazide and/or iso-nicotinohydrazide (0.01 mol) were added and then 5 drops glacial acetic acid was added as a catalyst. The reaction mixture was refluxed for 8 h. After completion of the reaction, the mixture was allowed to cool. The formed solid was obtained by filtration, washed with water, air dried and recrystallized from absolute ethanol to afford the corresponding derivatives (**2a–g**) respectively.

*4.1.2.1. N′-(1-[4-{(4-[4-Chlorophenyl]phthalazin-1-yl)amino}phenyl]ethylidene)benzohydrazide (**2a**).* Light brown crystals; yield, 70%; mp 260–2 °C; $IR_{\nu_{max}}$ (cm^{-1}): 3431 (NH), 2917 (CH aromatic), 2851 (CH aliphatic), 1617 (C=O), 1537 (C=N); ^1H NMR (400 MHz, DMSO-d_6) δ 10.88 (s, 1H), 9.21 (s, 1H), 8.26–7.51 (m, 17H), 2.51 (d, J = 34.4 Hz, 3H); ^{13}C NMR (101 MHz, DMSO-d_6) δ 197.12, 152.82, 152.29, 135.75, 135.46, 134.59, 133.31, 132.31, 132.27, 129.92, 129.45, 129.35, 129.20, 128.82, 128.24, 127.98, 127.42, 125.44, 121.71, 121.38, 27.05; MS (*m*/*z*): 493.1513 (M^+ + 2, 16.41%), 491.1513 (M^+, 49.68%), 485.28 (100%, base peak); Anal. calcd For $C_{29}H_{22}ClN_5O$ (491.98): C, 70.80; H, 4.51; N, 14.24. Found: C, 71.06; H, 4.59; N, 14.43%.

*4.1.2.2. 2-Bromo-N′-(1-[4-{(4-[4-chlorophenyl]phthalazin-1-yl)amino}phenyl]ethylidene)benzohydrazide (**2b**).* Yellowish brown crystals; yield, 74%; mp 265–7 °C; $IR_{\nu_{max}}$ (cm^{-1}): 3300, 3430 (NH), 3060 (CH aromatic), 2917 (CH aliphatic), 1659 (C=O), 1505 (C=N); ^1H NMR (400 MHz, DMSO-d_6) δ 10.99 (s, 1H), 8.82 (s, 1H), 8.76–8.74 (m, 2H), 8.16–8.12 (m, 2H), 8.10–8.02 (m, J = 6.9, 3H), 7.95 (d, J = 8.5 Hz, 2H), 7.83 (d, J = 8.4 Hz, 1H), 7.81–7.73 (m, 2H), 7.70–7.64 (m, 2H), 7.58–7.38 (m, 2H), 2.36 (s, 3H); ^{13}C NMR (101 MHz, DMSO-d_6) δ 196.90, 170.74, 164.82, 139.51, 138.43, 134.67, 132.38, 132.11, 132.06, 131.70, 130.80, 130.03, 129.85, 129.19, 129.12, 127.63, 126.94, 126.57, 123.90, 120.05, 26.93, 15.00, 14.06; MS (*m*/*z*): 571.0618 (M^+ + 2, 63.72%), 569.0618 (M^+, 64.90%), 419.23 (100%, base peak); Anal. calcd for $C_{29}H_{21}BrClN_5O$ (570.88): C, 61.01; H, 3.71; N, 12.27. Found: C, 60.89; H, 3.84; N, 12.50%.

*4.1.2.3. 2-Chloro-N′-(1-[4-{(4-[4-chlorophenyl]phthalazin-1-yl)amino}phenyl]ethylidene)benzohydrazide (**2c**).* Dark yellow powder; yield, 73%; mp 255–7 °C; $IR_{\nu_{max}}$ (cm^{-1}): 3422 (NH), 3209 (CH aromatic), 2918 (CH aliphatic), 1658 (C=O), 1594 (C=N); ^1H NMR (400 MHz, DMSO-d_6) δ 11.26 (s, 1H), 9.04 (s, 1H), 8.13–8.05 (m, 2H), 7.98–7.92 (m, 3H), 7.80–7.69 (m, 5H), 7.61–7.45 (m, 6H), 2.32 (s, 3H); ^{13}C NMR (101 MHz, DMSO-d_6) δ 170.09, 163.46, 154.82, 148.48, 137.32, 136.27, 135.08, 133.83, 132.18,

131.61, 130.78, 130.20, 130.07, 129.32, 129.27, 129.02, 127.74, 127.06, 126.89, 122.62, 122.39, 120.54, 15.03; MS (*m*/*z*): 527.1123 (M^+ + 2, 16.06%), 525.1123 (M+, 23.74%), 313.06 (100%, base peak); Anal. calcd For $C_{29}H_{21}Cl_2N_5O$ (526.42): C, 66.17; H, 4.02; N, 13.30. Found: C, 65.98; H, 4.18; N, 13.42%.

*4.1.2.4. N′-(1-[4-{(4-[4-Chlorophenyl]phthalazin-1-yl)amino} phenyl]ethylidene)-2-hydroxybenzohydrazide (**2d**).* Orange powder; yield, 75%; mp 262–4 °C; $IR_{\nu_{max}}$ (cm^{-1}): 3771 (OH), 3432 (NH), 2917 (CH aromatic), 2850 (CH aliphatic), 1650 (C=O), 1609 (C=N); ^1H NMR (400 MHz, DMSO-d_6) δ 11.81 (s, 1H), 11.31 (s, 1H), 9.53 (s, 1H), 8.73 (d, J = 8.4 Hz, 1H), 8.71–8.12 (m, 8H), 7.74 (d, J = 8.1 Hz, 2H), 7.66 (d, J = 8.2 Hz, 2H), 7.44 (t, J = 7.7 Hz, 1H), 7.06–6.99 (m, 2H), 2.38 (s, 3H); ^{13}C NMR (101 MHz, DMSO-d_6) δ 162.47, 157.07, 153.22, 152.98, 152.30, 142.43, 136.01, 134.04, 133.77, 132.95, 132.02, 131.87, 130.97, 129.02, 127.33, 126.16, 123.29, 120.46, 120.14, 119.07, 118.39, 117.36, 14.20; MS (*m*/*z*): 509.1462 (M^+ + 2, 5.77%), 507.1462 (M^+, 9.27%), 314.22 (100%, base peak); Anal. calcd for $C_{29}H_{22}ClN_5O_2$ (507.98): C, 68.57; H, 4.37; N, 13.79. Found: C, 68.73; H, 4.50; N, 14.06%.

*4.1.2.5. 4-Amino-N′-(1-[4-{(4-[4-chlorophenyl]phthalazin-1-yl) amino}phenyl]ethylidene)benzohydrazide (**2e**).* Reddish yellow powder; yield, 65%; mp 250–2 °C; $IR_{\nu_{max}}$ (cm^{-1}): 3726, 3674, 3446 (NH, NH_2), 3047 (CH aromatic), 2958 (CH aliphatic), 1628 (C=O), 1536 (C=N); ^1H NMR (400 MHz, DMSO-d_6) δ 10.42 (s, 1H), 9.16 (s, 1H), 8.22 (d, J = 7.9 Hz, 2H), 8.16–8.09 (m, 4H), 8.04 (m, 2H), 7.99–7.74 (m, 8H), 6.76 (d, J = 8.0 Hz, 2H), 2.40 (s, 3H); ^{13}C NMR (101 MHz, DMSO-d_6) δ 197.04, 166.48, 153.12, 152.66, 144.50, 132.25, 132.23, 130.07, 129.84, 129.39, 129.26, 127.69, 127.27, 125.37, 124.64, 123.50, 121.22, 120.53, 114.51, 113.48, 25.42; MS (*m*/*z*): 508.1622 (M^+ + 2, 4.00%), 506.1622 (M^+, 11.31%), 263.63 (100%, base peak); Anal. calcd for $C_{29}H_{23}ClN_6O$ (506.99): C, 68.70; H, 4.57; N, 16.58. Found: C, 68.94; H, 4.65; N, 16.80%.

*4.1.2.6. N′-(1-[4-{(4-[4-Chlorophenyl]phthalazin-1-yl)amino} phenyl]ethylidene)nicotinohydrazide (**2f**).* Brown powder; yield, 72%; mp 260–2 °C; $IR_{\nu_{max}}$ (cm^{-1}): 3429, 3248 (NH), 3090 (CH aromatic), 2918 (CH aliphatic), 1641 (C=O), 1536 (C=N); ^1H NMR (400 MHz, DMSO-d_6) δ 11.09 (s, 1H), 8.99 (s, 1H), 8.77 (d, 1H), 8.31 (d, 1H), 8.10–7.92 (m, 7H), 7.72–7.60 (m, 7H), 2.42 (s, 3H); ^{13}C NMR (101 MHz, DMSO-d_6) δ 196.90, 164.87, 162.80, 156.43, 152.69, 152.42, 148.99, 136.58, 134.94, 133.65, 132.14, 129.24, 129.14, 127.76, 127.21, 126.79, 124.46, 124.09, 122.20, 120.40, 120.33, 15.18; MS (*m*/*z*): 494.1465 (M^+ + 2, 0.77%), 492.1465 (M^+, 2.07%), 298.12 (100%, base peak); Anal. calcd for $C_{28}H_{21}ClN_6O$ (492.97): C, 68.22; H, 4.29; N, 17.05. Found: C, 68.43; H, 4.56; N, 17.24%.

*4.1.2.7. N′-(1-[4-{(4-[4-Chlorophenyl]phthalazin-1-yl)amino} phenyl]ethylidene)isonicotinohydrazide (**2g**).* Light brown powder, yield, 79%; mp 261–3 °C; $IR_{\nu_{max}}$ (cm^{-1}): 3429, 3248 (NH), 3090 (CH aromatic), 2918 (CH aliphatic), 1641 (C=O), 1536 (C=N); ^1H NMR (400 MHz, DMSO-d_6) δ 11.24 (s, 1H), 9.17 (s, 1H), 8.83 (m, 2H), 8.18–8.10 (m, 2H), 7.96 (m, 6H), 7.74–7.70 (m, 6H), 2.44 (s, 3H); ^{13}C NMR (101 MHz, DMSO-d_6) δ 197.01, 162.61, 157.42, 152.51, 150.63, 149.70, 148.35, 142.56, 140.01, 135.42, 134.94, 132.23, 129.87, 128.01, 127.79, 125.01, 123.07, 122.85, 120.94, 15.36; MS (*m*/*z*): 492.1465 (M^+, 3.13%), 76.34 (100%, base peak); Anal. calcd for $C_{28}H_{21}ClN_6O$ (492.97): C, 68.45; H, 4.29; N, 17.05. Found: C, 68.43; H, 4.47; N, 17.29%.

4.1.3. General procedure for the synthesis of compounds (3a–c). To a 100 ml round-bottom flask with a magnetic stirrer, compound (**1**) (3.73 g, 0.01 mol) was added in 50 ml absolute ethanol. Appropriate thiosemicarbazides, 4-phenyl-3-thiosemicarbazide and/or methyl hydrazinecarbodithioate (0.01 mol), were added and then 5 drops of glacial acetic acid was added as a catalyst. The reaction mixture was refluxed for 8 h. After completion of the reaction, the mixture was allowed to cool. The formed solid was obtained by filtration, washed with water, air dried and recrystallized from absolute ethanol to afford the corresponding derivatives (**3a–c**).

*4.1.3.1. 2-(1-[4-{(4-[4-Chlorophenyl]phthalazin-1-yl)amino} phenyl]ethylidene)hydrazine-1-carbothioamide (**3a**).* Light brown powder; yield, 70%; mp 203–5 °C; $IR_{\nu_{max}}$ (cm^{-1}): 3858, 3739, 3440 (NH, NH_2), 3055 (CH aromatic), 2918 (CH aliphatic), 1595 (C=N), 1402 (C=S); ^1H NMR (300 MHz, DMSO-d6) δ 11.11 (s, 1H), 9.04 (s, 1H), 8.20 (d, 2H), 8.07 (d, 2H), 8.00 (d, 2H), 7.82 (d, 2H), 7.74–7.69 (m, 4H), 6.55 (s, 2H), 2.23 (s, 3H); MS (*m*/*z*): 446.1080 (M^+, 12.05%), 444.1080 (M^+ - 2, 19.43%), 292.42 (100%, base peak); Anal. calcd for $C_{23}H_{19}ClN_6S$ (446.96): C, 61.81; H, 4.28; N, 18.80. Found: C, 61.97; H, 4.42; N, 18.95%.

*4.1.3.2. 2-(1-[4-{(4-[4-Chlorophenyl]phthalazin-1-yl)amino} phenyl]ethylidene)-N-phenylhydrazine-1-carbothioamide (**3b**).* Brown powder; yield, 66%; mp 243–5 °C; $IR_{\nu_{max}}$ (cm^{-1}): 3424 (NH), 2918 (CH aromatic), 2850 (CH aliphatic), 1623 (C=N), 1406 (C=S); ^{13}C NMR (101 MHz, DMSO-d_6) δ 166.02, 159.72, 152.87, 145.83, 142.18, 139.80, 138.80, 135.52, 134.50, 132.27, 131.69, 129.27, 128.32, 127.82, 126.88, 124.83, 122.59, 120.85, 115.26, 113.45, 12.24; MS (*m*/*z*): 522.1393 (M^+, 28.63%), 422.47 (100%, base peak); Anal. calcd for $C_{29}H_{23}ClN_6S$ (523.06): C, 66.59; H, 4.43; N, 16.07. Found: C, 66.38; H, 4.51; N, 16.23%.

*4.1.3.3. Methyl 2-(1-[4-{(4-[4-chlorophenyl]phthalazin-1-yl) amino}phenyl]ethylidene)hydrazine-1-carbodithioate (**3c**).* Yellow powder; yield, 70%; mp 205–7 °C; $IR_{\nu_{max}}$ (cm^{-1}): 3435 (NH), 3050 (CH aromatic), 2917 (CH aliphatic), 1591 (C=N), 1404 (C=S); ^1H NMR (300 MHz, DMSO-d6) δ 10.33 (s, 1H), 8.86 (s, 1H), 8.23–7.97 (m, 6H), 7.78–7.62 (m, 6H), 2.58 (s, 3H), 2.49 (s, 3H); ^{13}C NMR (101 MHz, DMSO-d_6) δ 197.02, 157.74, 153.21, 152.62, 144.53, 135.12, 134.21, 133.90, 132.23, 129.88, 127.44, 126.84, 125.27, 124.38, 123.75, 121.14, 27.00, 13.69; MS (*m*/*z*): 477.0849 (M^+, 12.81%), 368.38 (100%, base peak); Anal. calcd for $C_{24}H_{20}ClN_5S_2$ (478.03): C, 60.30; H, 4.22; N, 14.65. Found: C, 60.49; H, 4.37; N, 14.88%.

4.1.4. General procedure for the synthesis of 1-(4-[{4-(4-chlorophenyl)phthalazin-1-yl}oxy]phenyl)-3-phenylurea and/or thiourea (4a,b). To a 100 ml round-bottom flask with a magnetic stirrer, equimolar amounts of 1-chloro-4-(4-chlorophenyl)phthalazine (2.74 g, 0.01 mol) and the appropriate 1-(4-hydroxyphenyl)-3-phenylurea and/or thiourea (0.01 mol) were added in 50 ml DMF and then potassium carbonate anhydrous (0.01 mol) was added. The reaction mixture was heated in a water bath for 4 h. After completion of the reaction, the solid formed was filtered, washed several times with water and air dried to give the corresponding urea and/or thiourea derivatives **4a,b** respectively.

*4.1.4.1. 1-(4-[{4-(4-Chlorophenyl)phthalazin-1-yl}oxy]phenyl)-3-phenylurea (**4a**).* White solid; yield, 72%; mp 261–3 °C; $IR_{\nu_{max}}$ (cm^{-1}): 3440, 3304 (NH), 3078 (CH aromatic), 2919 (CH aliphatic), 1642 (C=O), 1600 (C=N), 1211 (C–O); ^1H NMR (300 MHz, DMSO-d_6) δ 9.76 (s, 1H), 9.15 (s, 1H), 8.53–8.45 (m, 1H), 8.18–8.01 (m, 3H), 7.96 (d, J = 7.5 Hz, 2H), 7.78–7.68 (m, 4H), 7.64 (dd, J = 8.6, 3.6 Hz, 4H), 7.27 (q, J = 6.3 Hz, 3H); MS (*m*/*z*): 466.1197 (M^+, 12.38), 301.62 (100%, base peak); Anal. calcd for $C_{27}H_{19}ClN_4O_2$ (466.93): C, 69.45; H, 4.10; N, 12.00. Found: C, 69.68; H, 4.21; N, 12.17%.

*4.1.4.2. 1-(4-[{4-(4-Chlorophenyl)phthalazin-1-yl}oxy]phenyl)-3-phenylthiourea (**4b**).* White solid; yield, 75%; mp 251–3 °C; $IR_{\nu_{max}}$ (cm^{-1}): 3421 (NH), 3068 (CH aromatic), 2919 (CH aliphatic), 1631 (C=N), 1403 (C=S), 1205 (C–O); MS (*m*/*z*): 482.0968 (M^+, 8.65), 312.46 (100%, base peak); Anal. calcd for $C_{27}H_{19}ClN_4OS$ (482.99): C, 67.14; H, 3.97; N, 11.60. Found: C, 67.50; H, 4.13; N, 11.68%.

4.1.5. General procedure for the synthesis of compounds (5a–d). To a 100 ml round-bottom flask with a magnetic stirrer, equimolar amounts of 1-chloro-4-(4-chlorophenyl)phthalazine (2.74 g, 0.01 mol) and the appropriate amide derivatives, namely, *N*-(4-hydroxyphenyl)acetamide, *N*-(4-hydroxyphenyl) benzamide, *N*-(4-hydroxyphenyl)-3-nitrobenzamide and/or *N*-(4-hydroxyphenyl)cinnamamide (0.01 mol) were added in 50 ml DMF. Then equimolar potassium carbonate anhydrous (0.01 mol) was added and the reaction mixture was heated in a water bath for 6 h. After completion of the reaction, the solid formed was filtered, washed several times with water and air dried to afford the corresponding compounds **5a–d** respectively.

*4.1.5.1. N-(4-[{4-(4-Chlorophenyl)phthalazin-1-yl}oxy]phenyl) acetamide (**5a**).* White solid; yield, 70%; mp 190–2 °C; $IR_{\nu_{max}}$ (cm^{-1}): 3316 (NH), 3067 (CH aromatic), 2970, 2919 (CH aliphatic), 1664 (C=O), 1606 (C=N), 1379 (C=S), 1201 (C–O); ^1H NMR (300 MHz, DMSO-d6) δ 10.03 (s, 1H), 8.14–7.93 (m, 4H), 7.72–7.63 (m, 6H), 7.31–7.28 (d, J = 8.7 Hz, 2H), 2.07 (s, 3H); MS (*m*/*z*): 389.0931 (M^+, 18.67), 264.11 (100%, base peak); Anal. calcd for $C_{22}H_{16}ClN_3O_2$ (389.84): C, 67.78; H, 4.14; N, 10.78. Found: C, 67.61; H, 4.25; N, 11.06%.

*4.1.5.2. N-(4-[{4-(4-Chlorophenyl)phthalazin-1-yl}oxy]phenyl) benzamide (**5b**).* Grey powder; yield, 68%; mp 245–7 °C; $IR_{\nu_{max}}$ (cm^{-1}): 3440 (NH), 3058 (CH aromatic), 2917 (CH aliphatic), 1650 (C=O), 1578 (C=N), 1202 (C–O); MS (*m*/*z*): 451.1088 (M^+, 5.43), 120.14 (100%, base peak); Anal. calcd for $C_{27}H_{18}ClN_3O_2$ (451.91): C, 71.76; H, 4.01; N, 9.30. Found: C, 71.53; H, 4.20; N, 9.47%.

*4.1.5.3. N-(4-[{4-(4-Chlorophenyl)phthalazin-1-yl}oxy]phenyl)-3-nitrobenzamide (**5c**).* Pale white powder; yield, 70%; mp 242–4 °C; $IR_{\nu_{max}}$ (cm^{-1}): 3427 (NH), 3073 (CH aromatic), 2917 (CH aliphatic), 1647 (C=O), 1527 (C=N), 1380 (NO_2), 1202 (C–O); ^1H NMR (300 MHz, DMSO-d6) δ 8.84 (d, J = 2.5 Hz, 1H), 8.53–8.41 (m, 3H), 8.11 (dt, J = 17.3, 7.2 Hz, 2H), 7.97 (d, J = 7.9 Hz, 1H), 7.87 (dd, J = 12.3, 8.0 Hz, 3H), 7.72 (d, J = 8.1 Hz, 3H), 7.66 (d, J = 8.4 Hz, 2H), 7.38 (d, J = 8.2 Hz, 2H); MS (*m*/*z*): 496.0938 (M^+, 3.14), 41.42 (100%, base peak); Anal. calcd for $C_{27}H_{17}ClN_4O_4$ (496.91): C, 65.26; H, 3.45; N, 11.28. Found: C, 65.50; H, 3.62; N, 11.44%.

*4.1.5.4. N-(4-[{4-(4-Chlorophenyl)phthalazin-1-yl}oxy]phenyl) cinnamamide (**5d**).* Light brown solid; yield, 78%; mp 248–9 °C; $IR_{\nu_{max}}$ (cm^{-1}): 3423 (NH), 3060 (CH aromatic), 2965, 2918 (CH aliphatic), 1653 (C=O), 1618 (C=C), 1572 (C=N), 1202 (C–O); ^1H NMR (300 MHz, DMSO-d6) δ 10.35 (s, 1H), 8.50 (d, J = 7.8 Hz, 1H), 8.15–8.05 (m, 2H), 7.96 (d, J = 8.0 Hz, 1H), 7.84–7.59 (m, 8H), 7.46–7.35 (m, 6H), 6.87 (d, J = 15.8 Hz, 1H). MS (*m*/*z*): 477.1244 (M^+, 28.93), 468.93 (100%, base peak); Anal. calcd for $C_{29}H_{20}ClN_3O_2$ (477.95): C, 72.88; H, 4.22; N, 8.79. Found: C, 73.05; H, 4.39; N, 9.07%.

4.2. Biological testing

4.2.1. *In vitro* anti-cancer activity. Our derivatives were tested against two cell lines, Hep G2 and MCF-7, by a MTT colorimetric assay. Cell lines were cultured in an RPMI-1640 medium with 10% fetal bovine serum. Then 100 units per ml penicillin and 100 μg ml^{-1} streptomycin antibiotics were added at 37 °C in a 5% CO_2 incubator. The cell lines were seeded in a 96-well plate at a density of 1.0×10^4 cells per well at 37 °C for 48 h under 5% CO_2. After incubation, the cells were treated with different concentrations of synthesized compounds and incubated for 24 h. After 24 h of drug treatment, 20 μl of MTT solution at 5 mg ml^{-1} was added and incubated for 4 h. Dimethyl sulfoxide (DMSO) in a volume of 100 μl was added into each well to dissolve the purple formazan formed. The colorimetric assay was performed and the measurements were recorded at an absorbance wavelength of 570 nm using a plate reader (EXL 800, USA). The relative cell viability in percentage was calculated as (A_{570} of treated samples/A_{570} of untreated sample) × 100. The results for IC_{50} values of the active compounds are summarized in Table 1.[35–37]

4.2.2. *In vitro* VEGFR-2 assay. The VEGFR-2 kinase activity was measured with an anti-phosphotyrosine antibody using an Alpha Screen system (PerkinElmer, USA) according to the manufacturer's instructions.[38] Enzyme reactions were performed with 50 mM Tris–HCl, pH 7.5, 5 mM $MnCl_2$, 5 mM $MgCl_2$, 0.01% Tween-20 and 2 mM DTT, containing 10 μM ATP, 0.1 μg ml^{-1} biotinylated poly-GluTyr (4 : 1) and 0.1 nM of VEGFR-2 (Millipore, UK). Prior to catalytic initiation with ATP, the tested compounds at final concentrations ranging from 0 to 300 μg ml^{-1} and enzyme were incubated at room temperature for 5 min. The reactions were quenched by the addition of 25 μl of 100 mM EDTA, 10 μg ml^{-1} Alpha Screen streptavidin donor beads and 10 μg ml^{-1} acceptor beads in 62.5 mM HEPES pH 7.4, 250 mM NaCl, and 0.1% BSA. The plate was left to incubate in the darkness overnight and then analyzed using an ELISA reader (PerkinElmer, USA). Control reactions were conducted with wells containing the substrate and enzyme without compounds, while wells containing biotinylated poly-GluTyr (4 : 1) and the enzyme without ATP were used as basal controls. The percent inhibition was calculated by comparing the compounds treated to control incubations. The concentration of the test compound causing 50% inhibition (IC_{50}) was determined from the concentration–inhibition response curve (triplicate determinations). Sorafenib (Sigma-Aldrich, USA) was used as a standard VEGFR-2 inhibitor for comparison.

4.3. Docking studies

VEGFR-2 (PDB ID 4ASD)[40] was used in the Molsoft program to carry out all docking studies. Each experiment used the VEGFR-2 receptor complexes with the Ligand downloaded from the Brookhaven Protein Databank. The compounds were drawn as a 3D structure and their energies were minimized. The ligand was extracted from the binding site and the compounds discussed herein were docked into the active site.

4.4. Molecular dynamics simulation

The highly active derivatives **2g**, **3a**, **4a** and **5b** were simulated using molecular dynamics (MD) in VEGFR-2 with the help of GAFF2.[40,41] The molecular dynamics utilizes Amber's MM/GBSA.py script and the trajectory, the receptor-ligand binding energy was calculated.[40] The force field AMBERff14SB for the protein and ligand force fields were produced.[43]

4.5. ADMET profile

The *in silico* ADMET profile of the highly active derivatives **2g** and **4a** was predicted using pkCSM descriptor algorithm procedures.[44]

Data availability

The data supporting this article have been included as part of the ESI.†

Conflicts of interest

There is no interest to declare.

References

1 A. A. El-Helby, R. R. A. Ayyad, H. Sakr, K. El-Adl, M. M. Ali and F. Khedr, *Arch. Pharm.*, 2017, **350**(12), DOI: 10.1002/ardp.201700240.
2 A. A. El-Helby, H. Sakr, R. R. A. Ayyad, K. El-Adl, M. M. Ali and F. Khedr, *Anticancer Agents Med. Chem.*, 2018, **18**(8), 1184–1196, DOI: 10.2174/1871520618666180412123833.
3 H. S. Abulkhair, A. Turky, A. Ghiaty, H. E. A. Ahmed and A. H. Bayoumi, *Bioorg. Chem.*, 2020, **100**, 103899, DOI: 10.1016/j.bioorg.2020.103899.
4 A. Turky, A. H. Bayoumi, A. Ghiaty, A. S. El-Azab, A. A.-M. Abdel-Aziz and H. S. Abulkhair, *Bioorg. Chem.*, 2020, 104019, DOI: 10.1016/j.bioorg.2020.104019.
5 W. M. Eldehna, S. M. Abou-Seri, A. M. El Kerdawy, R. R. Ayyad, H. A. Ghabbour, M. M. Ali and D. A. Abou El Ella, *Eur. J. Med. Chem.*, 2016, **113**, 50–62, DOI: 10.1016/j.ejmech.2016.02.029.
6 T. L. Bush, M. Payton, S. Heller, *et al.*, *Mol. Cancer Ther.*, 2013, **12**(11), 2356–2366, DOI: 10.1158/1535-7163.MCT-12-1178.
7 M. Payton, T. L. Bush, G. Chung, B. Ziegler, P. Eden, P. McElroy, S. Ross, V. J. Cee, H. L. Deak, B. L. Hodous, H. N. Nguyen, P. R. Olivieri, K. Romero, L. B. Schenkel, A. Bak, M. Stanton, I. Dussault, V. F. Patel, S. Geuns-Meyer, R. Radinsky and R. L. Kendall, *Cancer Res.*, 2010, **70**(23), 9846–9854.
8 M. A. J. Duncton, E. L. P. Chekler, R. Katoch-Rouse, D. Sherman, W. C. Wong, L. M. Smith, J. K. Kawakami, A. S. Kiselyov, D. L. Milligan, C. Balagtas, Y. R. Hadari, Y. Wang, S. N. Patel, R. L. Rolster, J. R. Tonra, D. Surguladze, S. Mitelman, P. Kussie, P. Bohlen and J. F. Doody, *Bioorg. Med. Chem.*, 2009, **17**(2), 731–740.
9 M. A. J. Duncton, E. L. Piatnitski, R. Katoch-Rouse, L. M. Smith, A. S. Kiselyov, D. L. Milligan, C. Balagtas, W. C. Wong, J. Kawakamia and J. F. Doody, *Bioorg. Med. Chem. Lett.*, 2006, **16**(6), 1579–1581.
10 A. S. Kiselyov, V. V. Semenov and D. Milligan, *Chem. Biol. Drug Des.*, 2006, **68**, 308–313.
11 E. L. Piatnitski, M. A. J. Duncton, A. S. Kiselyov, R. Katoch-Rouse, D. Sherman, D. L. Milligan, C. Balagtas, W. C. Wong, J. Kawakamia and J. F. Doody, *Bioorg. Med. Chem. Lett.*, 2005, **15**(21), 4696–4698.
12 D.-Q. Xue, X.-Y. Zhang, C.-J. Wang, L.-Y. Ma, N. Zhu, P. He, K.-P. Shao, P.-J. Chen, Y.-F. Gu, X.-S. Zhang, C.-F. Wang, C.-H. Ji, Q.-R. Zhang and H.-M. Liu, *Eur. J. Med. Chem.*, 2014, **85**, 235–244.
13 V. J. Cee, L. B. Schenkel, B. L. Hodous, H. L. Deak, H. N. Nguyen, P. R. Olivieri, K. Romero, A. Bak, X. Be, S. Bellon, T. L. Bush, A. C. Cheng, G. Chung, S. Coats, P. M. Eden, K. Hanestad, P. L. Gallant, Y. Gu, X. Huang, R. L. Kendall, M. J. Lin, M. J. Morrison, V. F. Patel, R. Radinsky, P. E. Rose, S. Ross, J. Sun, J. Tang, H. Zhao, M. Payton and S. D. Geuns-Meyer, *J. Med. Chem.*, 2010, **53**, 6368–6377.
14 G. Bold, J. Frei, P. Traxler, K.-H. Altmann, H. Mett, D. R. Stover and J. M. Wood, *EP Pat.*, 98/00764, 1998.
15 G. Bold, K.-H. Altmann, J. Frei, M. Lang, P. W. Manley, P. Traxler, B. Wietfeld, J. Brüggen, E. Buchdunger, R. Cozens, S. Ferrari, P. Furet, F. Hofmann, G. Martiny-Baron, J. Mestan, J. Rosel, M. Sills, D. Stover, F. Acemoglu, E. Boss, € R. Emmenegger, L. Lasser, E. Masso, R. Roth, C. Schlachter, W. Vetterli, D. Wyss and € J. M. Wood, *J. Med. Chem.*, 2000, **43**, 2310e2323.
16 J. Dumas and J. A. Dixon, *Expert Opin. Ther. Pat.*, 2005, **15**, 647e658.
17 A. S. Kiselyov, M. Semenova, V. V. Semenov and E. L. Piatnitski, *Chem. Biol. Drug Des.*, 2006, **68**, 250–255.
18 J. C. Tille, J. Wood, S. J. Mandriota, C. Schnell, S. Ferrari, J. Mestan, Z. Zhu, L. Witte and M. S. Pepper, *J. Pharmacol. Exp. Ther.*, 2001, **299**, 1073e1085.
19 M. A. Abdullaziz, H. T. Abdel-Mohsen, A. M. El Kerdawy, F. A. F. Ragab, M. M. Ali, S. M. Abu-Bakr, A. S. Girgis and H. I. El Diwani, Design, synthesis, molecular docking and cytotoxic evaluation of novel 2-furybenzimidazoles as VEGFR-2 inhibitors, *Eur. J. Med. Chem.*, 2017, **136**, 315–329.
20 M. A. Abdelgawad, K. El-Adl, S. S. El-Hddad, M. M. Elhady, N. M. Saleh, M. M. Khalifa, F. Khedr, M. Alswah, A. A. Nayl and M. M. Ghoneim, Design, molecular docking, synthesis, anticancer and anti-hyperglycemic assessments of thiazolidine-2, 4-diones Bearing Sulfonylthiourea

Moieties as Potent VEGFR-2 Inhibitors and PPARγ Agonists, *Pharmaceuticals*, 2022, **15**, 226.

21 F. Khedr, M.-K. Ibrahim, I. H. Eissa, H. S. Abulkhair and K. El-Adl, Phthalazine-based VEGFR-2 inhibitors: Rationale, design, synthesis, *in silico*, ADMET profile, docking, and anticancer evaluations, *Arch. Pharm.*, 2021, e2100201, DOI: 10.1002/ardp.202100201.

22 A. K. B. Aljohani, K. El-Adl, B. Almohaywi, O. M. Alatawi, M. Alsulaimany, A. El-morsy, S. A. Almadani, H. Y. Alharbi, M. S. Aljohani, F. A. Abdulhaleem M, H. E. M. Osman and S. Mohamady, *RSC Adv.*, 2024, **14**, 7964–7980.

23 M. M. Ghorab, A. M. Soliman, K. El-Adl and N. S. Hanafy, New quinazoline sulfonamide derivatives as potential anticancer agents: Identifying a promising hit with dual EGFR/VEGFR-2 inhibitory and radiosensitizing activity, *Bioorg. Chem.*, 2023, **140**, 106791, DOI: 10.1016/j.bioorg.2023.106791.

24 M. A. El-Zahabi, H. Sakr, K. El-Adl, M. Zayed, A. S. Abdelraheem, S. I. Eissa, H. Elkady and I. H. Eissa, Design, synthesis, and biological evaluation of new challenging thalidomide analogs as potential anticancer immunomodulatory agents, *Bioorg. Chem.*, 2020, **104**, 104218, DOI: 10.1016/j.bioorg.2020.104218.

25 N. M. Saleh, M. S. A. El-Gaby, K. El-Adl and N. E. A. Abd El-Sattar, Design, green synthesis, molecular docking and anticancer evaluations of diazepam bearing sulfonamide moieties as VEGFR-2 inhibitors, *Bioorg. Chem.*, 2020, **104**, 104350, DOI: 10.1016/j.bioorg.2020.104350.

26 A. E. Abdallah, I. H. Eissa, A. B. M. Mehany, H. Sakr, A. Atwa, K. El-Adl and M. A. El-Zahabi, Immunomodulatory quinazoline-based thalidomide analogs: Design, synthesis, apoptosis and anticancer evaluations, *J. Mol. Struct.*, 2023, **1281**, 135164, DOI: 10.1016/j.molstruc.2023.135164.

27 N. S. Hanafy, N. A. A. M. Aziz, S. S. A. El-Hddad, M. A. Abdelgawad, M. M. Ghoneim, A. F. Dawood, S. Mohamady, K. El-Adl and S. Ahmed, Design, synthesis, and docking of novel thiazolidine-2,4-dione multitarget scaffold as new approach for cancer treatment, *Arch. Pharm.*, 2023, e2300137, DOI: 10.1002/ardp.202300137.

28 D. Adel, K. El-Adl, T. Nasr, T. M. Sakr and W. Zaghary, Pyrazolo[3,4-d]pyrimidine derivatives as EGFRT790M and VEGFR-2 dual TK inhibitors: Design, synthesis, molecular docking, ADMET profile and anticancer evaluations, *J. Mol. Struct.*, 2023, **1291**, 136047, DOI: 10.1016/j.molstruc.2023.136047.

29 H. Elkady, K. El-Adl, H. Sakr, A. S. Abdelraheem, S. I. Eissa and M. A. El-Zahabi, Novel promising benzoxazole/benzothiazole-derived immunomodulatory agents: Design, synthesis, anticancer evaluation, and *in silico* ADMET analysis, *Arch. Pharm.*, 2023, e2300097, DOI: 10.1002/ardp.202300097.

30 M. A. El-Zahabi, H. Elkady, H. Sakr, A. S. Abdelraheem, S. I. Eissa and K. El-Adl, Design, synthesis, anticancer evaluation, *in silico* docking and ADMET analysis of novel indole-based thalidomide analogs as promising immunomodulatory agents, *J. Biomol. Struct. Dyn.*, 2023, 1–18, DOI: 10.1080/07391102.2023.2187217.

31 M. Alsulaimany, K. El-Adl, A. K. B. Aljohani, H. Y. Alharbi, O. M. Alatawi, M. S. Aljohani, A. El-Morsy, S. A. Almadani, A. A. Alsimaree, S. A. Salama, D. E. Keshek and A. A. Mohamed, Design, synthesis, docking, ADMET and anticancer evaluations of *N*-alkyl substituted iodoquinazoline derivatives as dual VEGFR-2 and EGFR inhibitors, *RSC Adv.*, 2023, **13**(51), 36301–36321, DOI: 10.1039/d3ra07700d.

32 K. E. Anwer, S. S. A. El-Hddad, N. E. A. Abd El-Sattar, A. M. El-Morsy, F. Khedr, S. Mohamady, D. E. G. Keshek, S. A. Salama, K. El-Adl and N. S. Hanafy, Five and six membered heterocyclic rings endowed with azobenzene as dual EGFRT790M and VEGFR-2 inhibitors: design, synthesis, *in silico* ADMET profile, molecular docking, dynamic simulation and anticancer evaluations, *RSC Adv.*, 2023, **13**, 35321–35338, https://api.semanticscholar.org/CorpusID:265657522.

33 M. S. A. El-Gaby, M. A. M. Abdel Reheim, Z. S. M. Akrim, B. H. Naguib, N. M. Saleh, A. A. A. M. El-Adasy, K. El-Adl and S. Mohamady, *Drug Dev. Res.*, 2024, **85**(1), DOI: 10.1002/ddr.22143.

34 A. A. Mohamed, S. S. A. El-Hddad, A. K. B. Aljohani, F. Khedr, O. M. Alatawi, D. E. Keshek, S. Ahmed, M. Alsulaimany, S. A. Almadani, K. El-Adl and N. S. Hanafy, Iodoquinazoline-derived VEGFR-2 and EGFRT790M dual inhibitors: Design, synthesis, molecular docking and anticancer evaluations, *Bioorg. Chem.*, 2024, **143**, 107062, DOI: 10.1016/j.bioorg.2023.107062.

35 T. Mosmann, *J. Immunol. Methods*, 1983, **65**(1–2), 55–63.

36 D. A. Scudiero, R. H. Shoemaker, K. D. Paull, A. Monks, S. Tierney, T. H. Nofziger, M. J. Currens, D. Seniff and M. R. Boyd, *Cancer Res.*, 1988, **48**(17), 4827–4833.

37 F. M. Freimoser, C. A. Jakob, M. Aebi and U. Tuor, *Appl. Environ. Microbiol.*, 1999, **65**(8), 3727–3729.

38 S. M. Abou-Seri, W. M. Eldehna, M. M. Ali and D. A. A. El Ella, *Eur. J. Med. Chem.*, 2016, **107**, 165–179.

39 S. A. H. El-Feky, H. A. Abd El-Fattah, N. A. Osman, M. Imran and M. N. Zedan, *J. Chem. Pharm. Res.*, 2015, **7**(7), 1154–1166.

40 B. R. Miller III, T. D. J. McGee, J. M. Swails, N. Homeyer, H. Gohlke and A. E. Roitberg, MMPBSA.py: An efficient program for end-state free energy calculations, *J. Chem. Theory Comput.*, 2012, **8**(9), 3314–3321.

41 J. A. Maier, C. Martinez, K. Kasavajhala, L. Wickstrom, K. E. Hauser and C. Simmerling, ff14SB: improving the accuracy of protein side chain and backbone parameters from ff99SB, *J. Chem. Theory Comput.*, 2015, **11**(8), 3696–3713.

42 J. Wang, R. M. Wolf, J. W. Caldwell, P. A. Kollman and D. A. Case, Development and testing of a general amber force field, *J. Comput. Chem.*, 2004, **25**(9), 1157–1174.

43 S. El-Hddad, M. Sobhy, A. Ayoub and K. El-Adl, *In silico* molecular docking, dynamics simulation and repurposing of some VEGFR-2 inhibitors based on the SARS-CoV-2-main-protease inhibitor N3, *J. Biomol. Struct. Dyn.*, 2022, 1–15, DOI: 10.1080/07391102.2022.2148000.

44 D. E. V. Pires, T. L. Blundell and D. B. Ascher, pkCSM: Predicting Small-Molecule Pharmacokinetic and Toxicity

Properties Using Graph-Based Signatures, *J. Med. Chem.*, 2015, **58**, 4066, DOI: **10.1021/acs.jmedchem.5b00104**.

45 C. A. Lipinski, F. Lombardo, B. W. Dominy and P. J. Feeney, Experimental and computational approaches to estimate solubility and permeability in drug discovery and development settings, *Adv. Drug Delivery Rev.*, 2012, **64**, 4–17.

46 A. Beig, R. Agbaria and A. Dahan, Oral delivery of lipophilic drugs: the tradeoff between solubility increase and permeability decrease when using cyclodextrin-based formulations, *PLoS One*, 2013, **8**, e68237.